

Quadrupole Moments of Highly Deformed Structures in the $A \sim 135$ Region: Probing the Single-Particle Motion in a Rotating Potential

R. W. Laird,¹ F. G. Kondev,^{1,2} M. A. Riley,¹ D. E. Archer,³ T. B. Brown,¹ R. M. Clark,⁴ M. Devlin,⁵ P. Fallon,⁴ D. J. Hartley,^{1,6} I. M. Hibbert,⁷ D. T. Joss,⁸ D. R. LaFosse,⁵ P. J. Nolan,⁸ N. J. O'Brien,⁷ E. S. Paul,⁸ J. Pfohl,¹ D. G. Sarantites,⁵ R. K. Sheline,¹ S. L. Shepherd,⁸ J. Simpson,⁹ R. Wadsworth,⁷ M. T. Matev,⁶ A. V. Afanasjev,^{10,11} J. Dobaczewski,^{12,13} G. A. Lalazissis,^{10,13,14} W. Nazarewicz,^{6,12,15} and W. Satuła^{12,13}

¹Department of Physics, Florida State University, Tallahassee, Florida 32306

²Physics Division, Argonne National Laboratory, Argonne, Illinois 60439

³Lawrence Livermore National Laboratory, Livermore, California 94550

⁴Nuclear Science Division, Lawrence Berkeley National Laboratory, Berkeley, California 94720

⁵Department of Chemistry, Washington University, St. Louis, Missouri 63130

⁶Department of Physics and Astronomy, University of Tennessee, Knoxville, Tennessee 37996-1200

⁷Department of Physics, University of York, Heslington, York YO1 5DD, United Kingdom

⁸Oliver Lodge Laboratory, University of Liverpool, Liverpool L69 3BX, United Kingdom

⁹CLRC, Daresbury Laboratory, Daresbury, Warrington, WA4 4AD, United Kingdom

¹⁰Physik-Department der Technischen Universität München, D-85747, Garching, Germany

¹¹Laboratory of Radiation Physics, University of Latvia, Miera Strasse 31, LV2169 Salaspils, Latvia

¹²Institute of Theoretical Physics, Warsaw University, ul. Hoża 69, PL-00681 Warsaw, Poland

¹³Joint Institute for Heavy-Ion Research, Oak Ridge National Laboratory, P.O. Box 2008, Oak Ridge, Tennessee 37831

¹⁴Department of Theoretical Physics, Aristotle University of Thessaloniki, Gr-54006 Thessaloniki, Greece

¹⁵Physics Division, Oak Ridge National Laboratory, P.O. Box 2008, Oak Ridge, Tennessee 37831

(Received 29 October 2001; published 27 March 2002)

The latest generation γ -ray detection system, GAMMASPHERE, coupled with the Microball charged-particle detector, has made possible a new class of nuclear lifetime measurement. For the first time differential lifetime measurements free from common systematic errors for over 15 different nuclei (>30 rotational bands in various isotopes of Ce, Pr, Nd, Pm, and Sm) have been extracted at high spin within a single experiment. This comprehensive study establishes the effective single-particle transition quadrupole moments in the $A \sim 135$ light rare-earth region. Detailed comparisons are made with theoretical calculations using the self-consistent cranked mean-field theory which convincingly demonstrates the validity of the additivity of single-particle quadrupole moments in this mass region.

DOI: 10.1103/PhysRevLett.88.152501

PACS numbers: 21.10.Re, 21.10.Tg, 21.60.-n, 27.70.+q

Deformation is a common phenomenon for subatomic and mesoscopic systems with many degrees of freedom (e.g., atomic nuclei, molecules, atomic clusters, quantum dots). It appears in field theory (Higgs mechanism), in the physics of superconductors, in condensed matter physics, and other fields of physics. The fundamental microscopic mechanism leading to the existence of deformed configurations, *spontaneous symmetry breaking*, was first proposed by Jahn and Teller for molecules [1]. The basic element of the Jahn-Teller (JT) effect is the vibronic coupling between the collective excitations of the system and the single-particle motion, known in nuclear structure as the particle-vibration (PV) coupling [2,3]. Depending on the geometrical properties of the individual valence nucleon (i.e., anisotropy of its wave function), the PV coupling can result in polarization that can change the original deformation of the core. However, if residual interactions are present, they effectively reduce the magnitude of the JT coupling. In particular, pairing correlations in atomic nuclei give rise to a large energy gap which weakens deformation effects. As a result, nuclear ground-state configurations experience a weak JT (pseudo-JT) effect, whereas

the extreme JT effect can take place in excited nuclear systems such as high-spin states [4,5].

One of the most stunning observations in studies of rapidly rotating atomic nuclei is that due to the strong Coriolis force residual pairing correlations are significantly quenched at high angular momenta (see Ref. [6] and references therein). Another factor that contributes to the diminished role of residual correlations is the reduced single-particle level density at the Fermi surface due to the presence of strong shell effects at deformed shapes. The resulting deformed potentials give rise to magic numbers that appear just as strikingly, but at quite different N and Z values, as for spherical nuclei. Consequently, high-spin nuclear superdeformation is probably the clearest example of pure single-particle motion in a deformed potential [7,8] and is thus a wonderful laboratory to study the nuclear JT effect and the nuclear shape polarization.

In the $A \sim 135$ light rare-earth region, a variety of rotational sequences with characteristics consistent with highly deformed prolate shapes with quadrupole deformation of $\beta_2 \sim 0.30$ – 0.40 , compared with $\beta_2 \sim 0.20$ for normal ground-state deformations, have been observed

[9]. These studies have revealed that the existence of highly deformed bands is the result of an interplay between microscopic shell effects, such as the occurrence of large shell gaps and the involvement of specific key orbitals such as the $\nu i_{13/2}[660]_{\frac{1}{2}}$, $\pi g_{9/2}[404]_{\frac{9}{2}}$, and possibly $\nu(f_{7/2} + h_{9/2})[541]_{\frac{1}{2}}$ [10–16]. For representative single-particle diagrams, see Refs. [10,17]. In an attempt to obtain a consistent understanding of the deformation properties of different single-particle orbitals throughout the $A \sim 135$ mass region, a comprehensive lifetime experiment with measurements on over 15 different nuclei was performed. While such an approach has been exploited for several nuclei in the $A = 80$ [18], 135 [19], 150 [20,21], and 190 [22,23] highly or superdeformed regions, it has never been done before in such a global manner in a single experiment.

From the lifetimes, one can extract “differential” transition quadrupole moments $\delta Q_t(^A Z; c) \equiv Q_t(^A Z; c) - Q_t(\text{core})$, where c stands for the configuration of the band in the nucleus $^A Z$ and $Q_t(\text{core})$ is the transition quadrupole moment of the assumed core nucleus. According to the “additivity principle” proposed in Ref. [24], the quadrupole moment δQ_t can be expressed as a sum of individual contributions carried by individual particle and hole states which appear near the Fermi level:

$$\delta Q_t \approx \delta Q_t^{\text{SM}} = \sum_i q_t(i), \quad (1)$$

where i runs over the particles and holes with respect to the core configuration in the nucleus $^A Z$. The quantity $q_t(i)$ represents the effective single-particle transition quadrupole moment, i.e., the change of the total intrinsic moment which is induced on the whole nucleus by the given particle or hole. By measuring or calculating values of $Q_t(^A Z; c)$ for a number of nuclei and configurations, one can extract values of $q_t(i)$ and thus the quadrupole polarizabilities associated with individual orbitals.

The transition quadrupole moments for various highly deformed structures in the $A \sim 135$ region have been measured in separate past experiments using the Doppler-shift attenuation method (DSAM). However, conclusive comparisons between similar structures in different nuclei were limited because of systematic differences such as reaction choice, target retardation properties, and varying sidefeeding considerations. In the present study, these systematic uncertainties were greatly reduced because the large variety of different nuclei were produced under similar conditions and analyzed using the same techniques.

High-spin states of a variety of $A \sim 135$ nuclei ($Z = 58$ –62) were populated after fusion of a 173 MeV ^{35}Cl beam with an isotopically enriched 1 mg/cm² ^{105}Pd foil mounted on a 17 mg/cm² Au backing. The emitted γ rays were collected using the GAMMASPHERE spectrometer [25] and the evaporated charged particles were identified with the Microball [26] at the 88-Inch Cyclotron at the Lawrence Berkeley National Laboratory.

The DSAM, centroid-shift technique was used in several different ways. For the most intense bands, spectra were generated by summing gates on the cleanest, fully stopped transitions at the bottom of the band of interest and projecting the events onto the “forward” (31.7°, 37.4°) and “backward” (142.6°, 148.3°) axes. These spectra were then used to extract the fractional Doppler shift, $F(\tau)$. In addition, double gates were set on in-band “moving” transitions in any ring of detectors and data were incremented into angle specific spectra. For the most intense bands, Doppler-shifted coincidence gates were also set on the highest spin transitions, making it possible to eliminate the effects of sidefeeding for states lower in the cascade. A 10% increase in the deduced quadrupole moment was consistently found for the $\nu i_{13/2}$ configurations when using the latter method as compared to the value extracted by gating on the stopped transitions at the bottom of the band.

The intrinsic quadrupole moments were extracted from the experimental $F(\tau)$ values using the code FITTAU [22] where $F(\tau)$ curves were generated assuming the band had a constant Q_t value. Although the uncertainties in the stopping powers and the modeling of the sidefeeding may contribute an additional systematic error of 15%–20% in the absolute Q_t values, the relative values are considered to be accurate to a level of $\sim 5\%$ –10%. Such precision allows for the first time a clear differentiation between the quadrupole polarizability of different orbital configurations for a variety of N and Z values in this mass region.

For highly deformed configurations, the present results displayed in Table I (see also Ref. [27] for normal-deformed structures), especially when taken together with values for $^{131,132}\text{Ce}$ [19], extracted using an identical analysis procedure, clearly indicate that for structures involving the $\nu i_{13/2}$ orbital there is a systematic decrease in the deformation as a function of increasing Z and N ; see also Fig. 1. Furthermore, the important role played by the $\pi g_{9/2}[404]_{\frac{9}{2}}$ orbital is confirmed by the fact that the largest deformations are observed for the Ce isotopes ($Z = 58$) where this orbital lies above the Fermi surface [17]. Note that the mixed $\nu(f_{7/2} + h_{9/2})[541]_{\frac{1}{2}}$ orbital exhibits Q_t values intermediate between the highly deformed ($\nu i_{13/2}$ and $\pi g_{9/2}$) and normal deformed configurations which have $Q_t \sim 3.0$ –3.5 e b [27].

To obtain a quantitative understanding of the measured quadrupole moments, cranking calculations without pairing using two different self-consistent mean-field methods were performed, namely, the cranked Skyrme Hartree-Fock method (CSHF) [28] with the Skyrme parametrization SLy4 [29], and the cranked relativistic mean-field theory (CRMF) [30,31] with the parametrization NL1 [32]. For the details pertaining to the current theoretical calculations, see Ref. [33]. Large deformed energy gaps develop at high angular momentum for $Z = 58$ and $N = 73$ [10], and thus the lowest highly deformed $\nu(i_{13/2})$ intruder band in ^{131}Ce can be considered a (super)deformed core in the $A \sim 135$ mass region. In order to perform a reliable statistical analysis of individual quadrupole moments according

TABLE I. Transition quadrupole moments for highly deformed configurations measured in this work. Unless stated otherwise, Q_t values were deduced using the centroid-shift technique with Q_t (sidefeeding) = Q_t . The normal deformed structures display $Q_t \sim 3.0\text{--}3.5 e b$ [27].

Nucleus	Configuration ^a	$Q_t(e b)$	Ref.
¹³⁰ Pr	$\pi h_{11/2} \otimes \nu(f_{7/2} + h_{9/2})$ (band 1,2)	4.3(3),4.5(3) ^b	[13]
	$\pi g_{9/2} \otimes \nu h_{11/2}$	6.1(5)	[13]
¹³¹ Pr	$\pi g_{9/2}$	5.3(4)	[13]
¹³² Pr	$\pi h_{11/2} \otimes \nu(f_{7/2} + h_{9/2})$	4.1(3) ^b	[14]
	$\pi g_{9/2} \otimes \nu i_{13/2}$	7.0(7)	
¹³³ Nd	$\nu(f_{7/2} + h_{9/2})$ ($\alpha = +\frac{1}{2}, -\frac{1}{2}$)	4.2(3),4.1(3) ^b	
	$\nu i_{13/2}$	5.8(2),6.5(2) ^c	[15]
¹³⁵ Nd	$\nu i_{13/2}$	5.1(2),5.7(2) ^c	[15]
¹³³ Pm	$\pi g_{9/2}$	5.0(4)	
¹³⁴ Pm	$\pi h_{11/2} \otimes \nu(f_{7/2} + h_{9/2})$	3.9(2) ^b	
¹³⁶ Pm	$\pi h_{11/2} \otimes \nu i_{13/2}$ (band 1)	4.8(3),5.2(3) ^c	[16]
	$\pi h_{11/2} \otimes \nu i_{13/2}$ (band 2)	4.8(4),5.2(4) ^c	[16]
	$\pi g_{7/2} \otimes \nu i_{13/2}$ (band 1,2)	5.7(6),5.7(6)	[16]
¹³⁵ Sm	$\nu i_{13/2}$	5.8(4),6.4(4) ^d	
¹³⁷ Sm	$\nu i_{13/2}$	4.4(3),4.8(4) ^c	

^a $\pi g_{9/2}$: $[404]_{2}^{2+}$, $\pi h_{11/2}$: $[541]_{2}^{3-}$, $\pi g_{7/2}$: $[413]_{2}^{5+}$, $\nu h_{11/2}$: $[523]_{2}^{7-}$, $\nu(f_{7/2} + h_{9/2})$: $[541]_{2}^{1-}$, $\nu i_{13/2}$: $[660]_{2}^{1+}$.

^bNo appreciable difference in deduced Q_t when gating above or below the level of interest.

^cDeduced by gating above the level of interest, so that sidefeeding was eliminated.

^dAssumed similar sidefeeding time structure to other highly deformed $\nu i_{13/2}$ bands.

to Ref. [24], it was necessary to carry out calculations for a large number of nuclei and configurations: our data set consisted of 183 bands in CSHF and 105 bands in CRMF (see Table II).

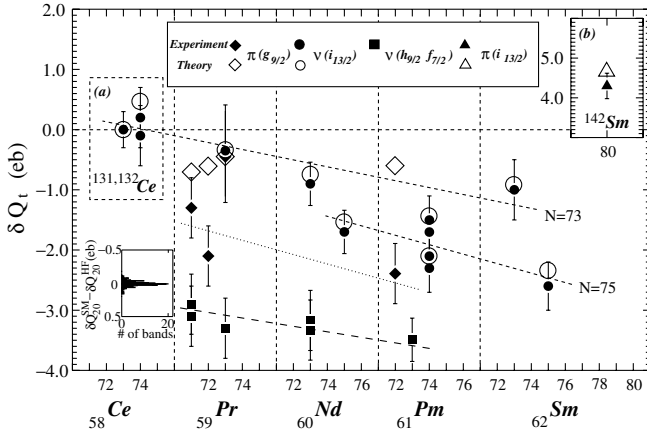


FIG. 1. Experimental (closed symbols with error bars) and calculated (CSHF, open symbols) differential transition quadrupole moments for Ce, Pr, Nd, Pm, and Sm nuclei as a function of neutron number. As a reference core, the highly deformed $\nu i_{13/2}$ band in ¹³¹Ce with experimental $Q_t = 7.4(3) e b$ [19] and theoretical (CSHF) $Q_t = 7.64 e b$ was assumed. The experimental values for ^{131,132}Ce and ¹⁴²Sm were taken from Refs. [19] and [21], respectively. Dashed lines are drawn simply to guide the eye. The inset in the bottom left-hand corner illustrates the distribution of differences between the single-particle sum δQ_{20}^{SM} and the HF value of δQ_{20}^{HF} for all the 183 bands considered in the statistical analysis of individual quadrupole moments. The distribution is sharply concentrated around zero and for the majority of bands the difference is less than $0.05 e b$. One can thus conclude that additivity works extremely well in the whole region discussed.

The transition quadrupole moment can be written as $Q_t = Q_{20} + \sqrt{\frac{2}{3}} Q_{22}$, where Q_{20} and Q_{22} are calculated components of the quadrupole moment [34]. Figure 1 shows the experimental and calculated CSHF values of $Q_t - Q_t(\text{core}) = \delta Q_t$ for the highly deformed bands in nuclei with $Z = 58\text{--}62$. The agreement between experiment and theory is quite remarkable. Theoretical values for bands attributed to the $\nu[541]1/2$ orbital are not shown in Fig. 1 since pairing correlations at the low observed spins effectively reduce the occupation of this mixed orbit. Pairing may also provide an explanation for the discrepancy observed for the $\pi g_{9/2}[404]_{2}^{2+}$ band in ¹³³Pm where the experimental measurements are at very low rotational frequencies ($\hbar\omega < 0.4$ MeV).

From the differential proton quadrupole moments δQ_{20}^{π} and δQ_{22}^{π} calculated at rotational frequency of $\hbar\omega = 0.65$ MeV, effective single-particle charge quadrupole moments $q_{20}(i)$ and $q_{22}(i)$ were extracted for protons and neutrons according to the additivity principle, Eq. (1) [with $q_t(i) = q_{20}(i) + \sqrt{\frac{2}{3}} q_{22}(i)$]. The results of the linear regression analysis for q_{20} are displayed in Table II. Note that the two models give very similar results. For tabulated values of q_{22} and effective angular momentum alignments and statistical errors, see Ref. [33].

The general trend of decreasing Q_t in the highly deformed structures with increasing Z and N in Fig. 1 is consistent with general expectations that, as one adds particles above a deformed shell gap, the stabilizing effect of the gap may be diminished. This trend continues until a new “magic” deformed number is reached or new superintruder orbitals become occupied. Such an event clearly occurs at $Z = 62$ and $N = 80$ (¹⁴²Sm) where a large jump

TABLE II. Effective charge quadrupole moments q_{20} (in $e b$) for single-particle orbitals [10,17] around a ^{131}Ce core. Particle states are labeled with an *. The orbitals are labeled by means of asymptotic quantum numbers $[Nn_z\Lambda]\Omega$ and the signature quantum number α . Note that in most cases the signature dependence is very weak.

Orbital	CSHF	CSHF	CRMF	CRMF
	$\alpha = -\frac{1}{2}$	$\alpha = +\frac{1}{2}$	$\alpha = -\frac{1}{2}$	$\alpha = +\frac{1}{2}$
Neutrons				
$[402]_{\frac{5}{2}}$	-0.35*	-0.33*	-0.26*	-0.26*
$[530]_{\frac{1}{2}}$	0.22*	0.17*	0.17*	0.19*
$[660]_{\frac{1}{2}}$	0.36*	0.38	0.36*	0.40
$[411]_{\frac{1}{2}}$	-0.15	-0.12	-0.11	-0.06
$[411]_{\frac{3}{2}}$	-0.15	-0.11	-0.13	-0.12
$[413]_{\frac{5}{2}}$	-0.13	-0.12	-0.13	-0.11
$[523]_{\frac{1}{2}}$	0.03	0.04	0.05	0.01
$[532]_{\frac{5}{2}}$	0.19	0.24	0.17	0.38
$[541]_{\frac{1}{2}}$	0.35	0.37	0.35	0.33
Protons				
$[404]_{\frac{9}{2}}$	-0.32*	-0.31*	-0.37*	-0.37*
$[532]_{\frac{5}{2}}$	0.43*	0.56*	0.41*	0.54*
$[422]_{\frac{3}{2}}$	0.33	0.34	0.33	0.28
$[541]_{\frac{3}{2}}$	0.50	0.57	0.48	0.50
$[550]_{\frac{1}{2}}$		0.49		0.47

in quadrupole moment marks the point at which it becomes energetically favorable to fill the high- j $\pi i_{13/2}$ and $\nu j_{15/2}$ orbitals creating the $A \sim 142$ superdeformed island; see the inset in Fig. 1. It is gratifying to see that our calculations can reproduce δQ_t in ^{142}Sm using *both* ^{131}Ce (this work) and ^{152}Dy (see Ref. [21]) cores.

In summary, it has been possible to extract differential transition quadrupole moments, free from common systematic errors for the largest number of different nuclei and configurations at high spin within a single experiment. This comprehensive study establishes Z , N , and configuration dependent quadrupole moment trends in the $A \sim 135$ light rare-earth region. Detailed comparisons are made with theoretical calculations using the cranked Skyrme Hartree-Fock and cranked relativistic mean-field frameworks. Remarkable agreement has been found for highly deformed intruder bands in this region up to ^{142}Sm demonstrating that the additivity of effective single-particle transition quadrupole moments works extremely well whether adding particles or holes to a ^{131}Ce or ^{152}Dy core, respectively.

Discussions with R. V. F. Janssens, D. Ward, and A. Galindo-Uribarri are greatly appreciated. The authors give special thanks to D. C. Radford and H. Q. Jin for software support. The authors thank the LBNL staff for their assistance during the experiment. This work was supported

in part by the U.S. Department of Energy under Contracts No. DE-FG02-96ER40963, No. DE-FG05-87ER40361, and No. DE-AC05-00OR22725, LLC (ORNL), the National Science Foundation, the State of Florida, and the U.K. Engineering and Physical Science Research Council. A. V. A. acknowledges support from the Alexander von Humboldt Foundation.

- [1] H. A. Jahn and E. Teller, Proc. R. Soc. London A **161**, 220 (1937).
- [2] A. Bohr, Mat. Fys. Medd. K. Dan. Vidensk. Selsk. **26**, No. 14 (1952).
- [3] A. Bohr and B. R. Mottelson, *Nuclear Structure* (Benjamin, New York, 1975), Vol. II.
- [4] P.-G. Reinhard and E. W. Otten, Nucl. Phys. **A420**, 173 (1984).
- [5] W. Nazarewicz, Int. J. Mod. Phys. E Suppl. **2**, 51 (1993); Nucl. Phys. **A574**, 27c (1994).
- [6] A. V. Afanasjev, D. B. Fossan, G. J. Lane, and I. Ragnarsson, Phys. Rep. **322**, 1 (1999).
- [7] G. de France, C. Baktash, B. Haas, and W. Nazarewicz, Phys. Rev. C **53**, R1070 (1996).
- [8] S. T. Clark *et al.*, Phys. Rev. Lett. **87**, 172503 (2001).
- [9] B. Singh, R. B. Firestone, and S. Y. F. Chu, Table of Superdeformed Nuclear Bands and Fission Isomers, LBL Report No. LBL-38004 (available at <http://ie.lbl.gov/sdband/cover.pdf>).
- [10] R. Wyss *et al.*, Phys. Lett. B **215**, 211 (1988).
- [11] A. Galindo-Uribarri *et al.*, Phys. Rev. C **50**, R2655 (1994); **54**, 1057 (1996).
- [12] A. Galindo-Uribarri *et al.*, Phys. Rev. C **54**, R454 (1996).
- [13] F. G. Kondev *et al.*, Eur. Phys. J. A **2**, 249 (1998).
- [14] F. G. Kondev *et al.*, Phys. Rev. C **59**, 3076 (1999).
- [15] F. G. Kondev *et al.*, Phys. Rev. C **60**, 011303 (1999).
- [16] J. Pfohl *et al.*, Phys. Rev. C **62**, 031304(R) (2000).
- [17] A. V. Afanasjev and I. Ragnarsson, Nucl. Phys. **A608**, 176 (1996).
- [18] F. Lerma *et al.*, Phys. Rev. Lett. **83**, 5447 (1999).
- [19] R. M. Clark *et al.*, Phys. Rev. Lett. **76**, 3510 (1996).
- [20] H. Savajols *et al.*, Phys. Rev. Lett. **76**, 4480 (1996).
- [21] G. Hackman *et al.*, Phys. Lett. B **416**, 268 (1998).
- [22] E. F. Moore *et al.*, Phys. Rev. C **55**, R2150 (1997).
- [23] B. C. Busse *et al.*, Phys. Rev. C **57**, R1017 (1998).
- [24] W. Satuła, J. Dobaczewski, J. Dudek, and W. Nazarewicz, Phys. Rev. Lett. **77**, 5182 (1996).
- [25] I. Y. Lee *et al.*, Nucl. Phys. **A520**, 641c (1990).
- [26] D. G. Sarantites *et al.*, Nucl. Instrum. Methods Phys. Res., Sect. A **381**, 418 (1996).
- [27] M. A. Riley *et al.*, Acta Phys. Pol. B **32**, 2683 (2001).
- [28] J. Dobaczewski and J. Dudek, Comput. Phys. Commun. **131**, 164 (2000).
- [29] E. Chabanat *et al.*, Nucl. Phys. **A635**, 231 (1998).
- [30] W. Koepf and P. Ring, Nucl. Phys. **A493**, 61 (1989); **511**, 279 (1990).
- [31] A. V. Afanasjev, J. König, and P. Ring, Nucl. Phys. **A608**, 107 (1996).
- [32] P.-G. Reinhard *et al.*, Z. Phys. A **323**, 13 (1986).
- [33] M. Matev *et al.* (to be published).
- [34] P. Ring *et al.*, Phys. Lett. **110B**, 423 (1982).